JOURNAL OF MATERIALS SCIENCE 37 (2002) 89–99

Friction-stir welding of a beryllium-aluminum powder metallurgy alloy

F. CONTRERAS, E. A. TRILLO, L. E. MURR
Department of Metallurgical and Materials Engineering, The University of Texas at El Paso, El Paso, TX 79968, USA

The friction-stir welding of a 62 Be-38 Al composite consisting of a Be phase in a continuous Al matrix produced a recrystallized, refined weld zone microstructure with intermixed, equiaxed grains of Be and Al, which increased in hardness by 43 percent from the base metal hardness. Like other friction-stir weld processes, there was no melting and no apparent release of airborne Be or BeO, rendering the process environmentally and technically attractive.

1. Introduction

There has been a considerable effort over the past decade to develop advanced manufacturing techniques for the fabrication of aluminum-intensive and other, related light-weight vehicles, particularly automobiles which have traditionally been made of steels. Concepts include aluminum or other light-weight space-frame design concepts which focus primarily on welding cast components and extruded lineals in truss configurations [1]. More recently, the idea of utilizing beryllium-aluminum alloys with high specific strength and stiffness in related structural designs has gained some interest especially since some current alloys have about 0.8 the density of aluminum and three times its stiffness; with excellent performance at elevated temperature [2]. Investment-cast Be-Al alloys, called Beralcast®, have historically been used primarily in aerospace applications such as the F-22 jet fighter, and Brush Wellman (Elmore, OH) currently produces a powder metallurgy product by gas atomization and consolidation by hot isostatic pressing (HIP) and cold isostatic pressing (CID); followed by extrusion or rolling processes [3]. This product, designated AlBeMet® AM 162 (nominally 62% Be and 38% Al) is used in aircraft and aerospace structural parts, and satellite avionics; as well as Formula One pistons in high performance race cars [3]. AlBeMet 162 is also characterized as a beryllium metal-matrix composite with demonstrated ability to meet design needs for a high modulus, high thermal conductivity, low density, and a tailorable coefficient of thermal expansion material [4].

Friction-stir welding (FSW) has also emerged as a novel joining process over the past decade and has been demonstrated to be especially effective in joining virtually any commercial 1xxx, 2xxx, 5xxx, 6xxx, and 7xxx aluminum alloy as well as virtually any dissimilar systems of these aluminum alloys, including those processed by casting, extrusion, rolling, etc. [4–11]; and aluminum (metal matrix composites (MMC's) such as Al 6061 + Al_2O_3 and A339 + SiC, etc. [5]. However, there are no reports of efforts to apply FSW to beryllium joining or the joining of Be-Al alloys where there may be significant health benefits as a consequence of eliminating toxic Be and BeO vapors, etc. because there is no melting associated with the FSW process.

In this research program we explore the FSW of rolled plate of AlBeMet® AM 162 (nominally 61.5% Be, 38.5% Al alloy) and examine the initial and residual (welded) microstructures utilizing light metallography and scanning and transmission electron microscopy.

2. Experimental details

Extruded, rolled plate of AlBeMet AM 1622 nominally 0.64 cm thick was friction-stir welded as illustrated schematically in Fig. 1 or the tool was inserted in a hole in a solid plate and stirring was achieved by traversing in the plate away from the hole. The butted workpiece plates were held in contact with one another on a steel backing plate. The head-pin (stirring tool) was a 1/4-20 carbon steel (right-handed) screw slightly shorter than the workpiece thickness; and held in a 1.9 cm diameter milling chuck. The tool was rotated counter-clockwise at a speed $R = 1000$ rpm; with a traverse speed $T = 1$ mm/s (Fig. 1). While no specific measurements of Be or BeO release were conducted, there was no visual or apparent vapor or other particulate release into the air at the weld region during the FSW process.

Vickers microhardness measurements were made by traversing through the base metal through the FSW zone near the mid section of a through-thickness illustrated schematically in Fig. 1 after cutting and polishing a representative sample. A 1 N (100 gf) load was utilized in a Shimadzu digital hardness tester.

The polishing procedures for the BeAl material were much the same as for many Al alloys. The grinding process utilized SiC papers that started from 80 grit down a series of 220, 320, 500, 800, and finally 1200 grit. Polishing consisted of a 1.0 and 0.3 micron size alumina slurry. Final polishing was performed by using colloidal silica. Great care was taken so that the BeAl particles

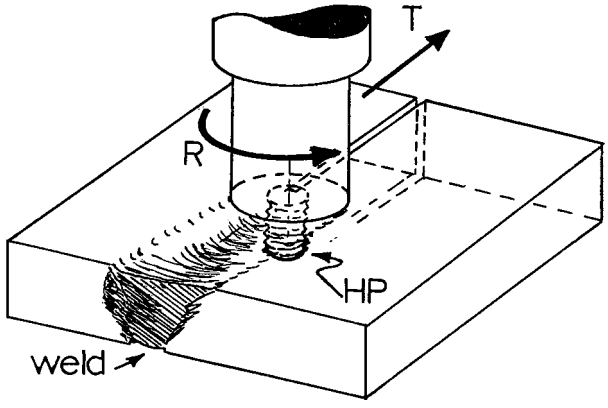

Figure 1 Schematic view of the friction-stir welding process. The rotating tool or head-pin (HP) is rotated at a speed R (rpm) while advancing along the butted plate interface at a rate of T (mm/s). A steel backing plate is placed beneath the butted plates to provide a stable platform for welding.

were thoroughly rinsed off the polishing cloths and surrounding area. Samples were etched using a Keller's solution that consisted of 1 mL HF, 1.5 mL HCl, 2.5 mL HNO_3, and 90 mL H_2O in an ice bath.

Thin specimens for transmission electron microscopy (TEM) were initially sliced from the workpieces and the FSW zone in the same manner as the polished and etched sections were prepared above for light metallography, but were ground to nominal thicknesses of 0.1 mm, and 3 mm discs were punched and mechanically dimpled on both sides of the discs. The 0.1 mm thickness was half the normal thickness for aluminum and its alloys. The disc specimens were then jet electropolished in a Tenupol-3 dual jet unit to produce electron transparent sections using 300 mL nitric acid in 1200 mL methanol; at –15°C. A Hitachi H-8000 analytical TEM employing a goniometer-tilt stage and fitted with a Noran energy-dispersive X-ray spectrometer was operated at an accelerating potential of 200 kV to examine the thin foil specimens.

3. Results and discussion

Fig. 2 illustrates the beryllium-aluminum metal matrix composite microstructure for the AlBeMet® AM 162 base plate in the thickness plane (viewed as in Fig. 1). The atomized, irregular, spherical-like Be particles and particle clusters are observed to be immersed in the aluminum as a continuous Al matrix binder. There is, as observed in the TEM bright-field image of Fig. 2b, little deformation within the polycrystalline Be particles or the aluminum matrix. It is apparent that the Be particles and particle agglomerates, which range in size from roughly 0.5 μm to 70 μm, have also occluded aluminum particles within them (arrows in Fig. 2a). The aluminum matrix binder is also generally polycrystalline with a grain size ranging from roughly 0.1 to 4 μm; essentially equiaxed. Regions of large crystallinity also occur in the Al matrix. For example the binder region between some Be particles is sometimes a continuous, crystal orientation. Fig. 2c illustrates the grains composing a polycrystalline Be particle or particle agglomerate as observed in the TEM. These grains are slightly smaller on average than the Al matrix binder grains. There are a few dislocations visible in the image (arrow). However the fact that the base metal exhibits little deformation microstructure is indicative of the PM process involved in the hot fabrication of the starting plate material.

It is interesting to note that the specific stiffness (E/ρ), (where E is the elastic modulus = 193 GPa and ρ is the corresponding density of 2.1 g-cm^{-3}) for the Be particles is 2.76 times that of the aluminum matrix (where $E = 70$ GPa and $\rho = 2.7$ g-cm^{-3}). While the Be agglomerates and the Al matrix binder appear to be somewhat uniform in terms of the composing grain sizes, the agglomerated, polycrystalline Be in the Al matrix binder creates the ideal features of a composite. That is, distinct regimes of varying modulus (elastic and shear).

Figs 3 to 5 show the FSW of the AM 162 plate represented in the microstructures in Fig. 2; along with the corresponding microstructures for comparison with Fig. 2. The weld features shown in Fig. 3a illustrate considerable weld discontinuity and weld tunnel formation on the right side (leading edge) or the tool advance side with an excellent weld on the left side (trailing edge) of the weld. The weld zone exhibits considerable dynamic recrystallization and especially refinement of the Be agglomerates to produce an overall, refined FSW zone microstructure in contrast to the starting base metal, especially prominent in Fig. 3b. This refined microstructure facilitates the necessary solid-state flow during welding as described for many other FSW systems previously [5–8]. It can be noted in Fig. 3b that the Be agglomerates become distorted (elongated) especially at the base-metal/FSW zone transition, which is actually very sharp. That is, the recrystallized FSW zone can be observed to contact several of the elongated Be agglomerates (arrows), and the FSW zone (at the lower right in Fig. 3b) can be observed to be a rather homogeneous, fine refinement, intermixing the aluminum matrix binder and the beryllium.

Although the weld bead in Fig. 3a is not technically good, the weld does exhibit some excellent prospects for welding this composite. Better welds may be achieved with very hard tools such as WC operating at much higher rotation speeds. These weld experiments will be undertaken in the future.

Fig. 4 illustrates the solid-state flow features through differential etching produced by compositional variations producing an intercalation of these compositionally different regimes. It is interesting to note in Fig. 4 that the initial Be agglomerates have been refined (recrystallized) to produce a much finer composite of recrystallized Be in the recrystallized aluminum matrix. Fig. 4a shows compositional lamellae which, although mixtures of very fine, recrystallized Be and Al, contain variations in the concentrations of Be and Al grains as determined from variations in the selected-area electron diffraction (SAD) patterns in TEM analyses to be described later. Fig. 4b and c illustrate these features in progressively higher magnifications of an area enclosed/dotted in both Fig. 4a and b. It is also significant to note the melting point difference between the aluminum matrix (~660°C) in contrast to the beryllium particles (~1300°C); essentially a factor of two.

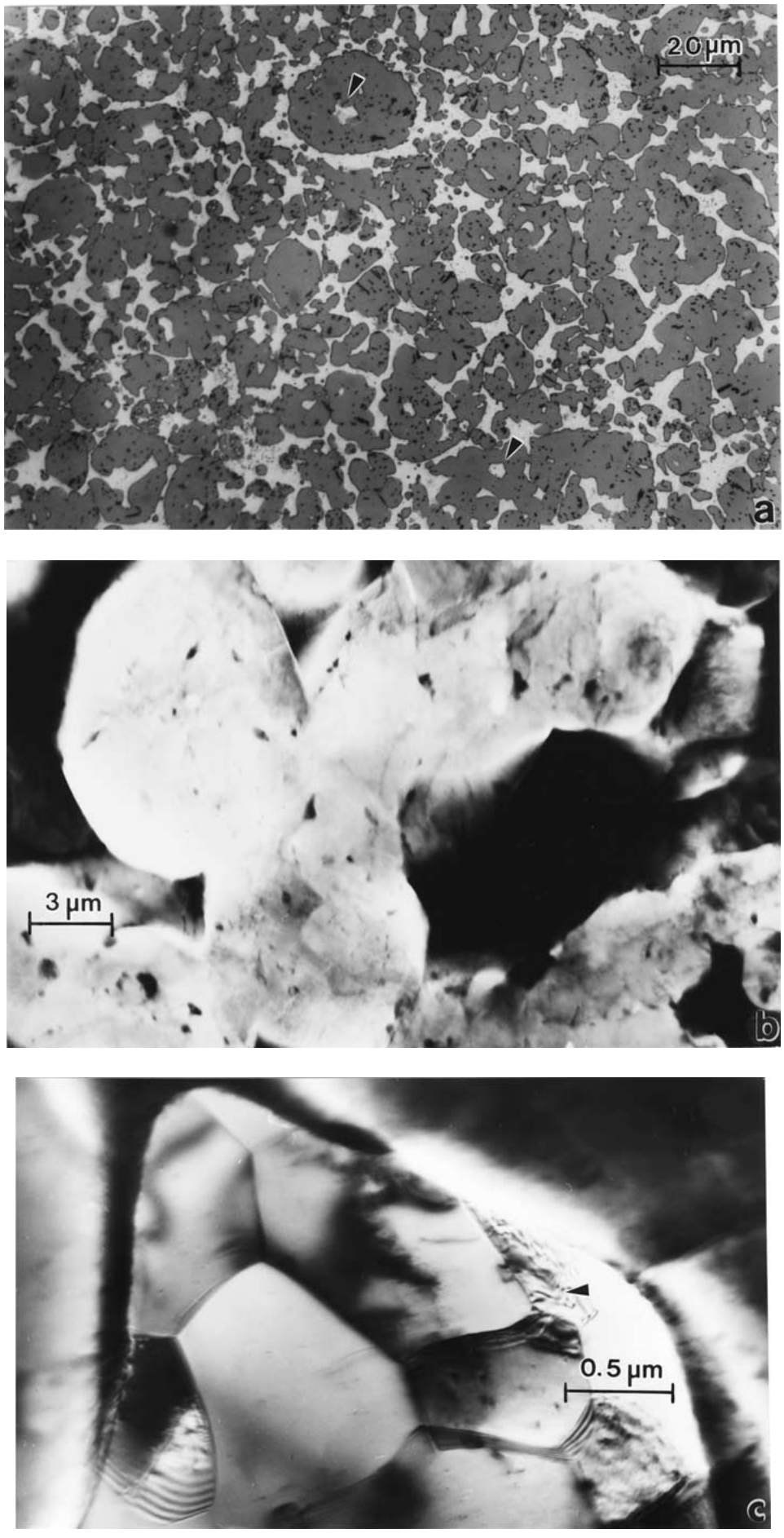

Figure 2 Optical metallographic (a) and TEM ((b) and (c)) views of the starting, Be 62-Al 38 base metal microstructures. (a) Typical microstructure view of Be phase particles in a continuous Al matrix. (b) TEM bright-field image showing the base metal component microstructures. (c) TEM bright-field image showing fine Be grains composing a Be aggregate/agglomerate.

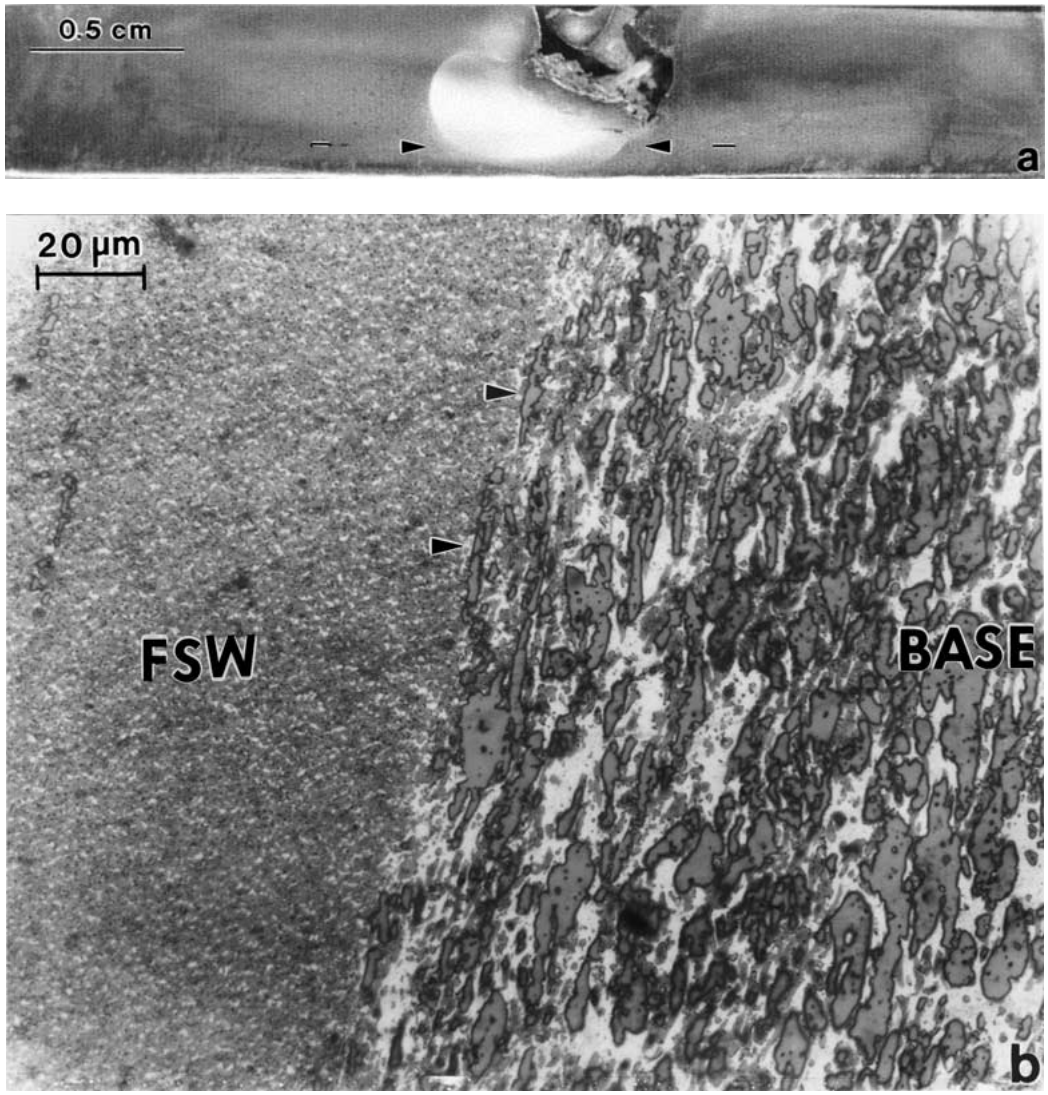

Figure 3 Example of FSW for the Be 62-Al 38 composite in a solid plate (a) and a metallographic comparison of the associated base/FSW microstructures as noted (b). The area in (b) corresponds to either the left region and the lower right at the base metal/weld zone interface. The arrows in (a) near the base indicate the general path for microhardness readings through the weld zone.

This is also characteristic of the respective recrystallization temperatures which are nominally half the melting point.

Fig. 5 shows, for comparison with base metal microstructures shown in Fig. 2b and c, the TEM microstructures near the transition region at the base metal/FSW interface or transition region where there is some noticeable deformation, as implicit in the interface region in Fig. 3b. The Be particles continue to exhibit little or no dislocation substructure while the Al matrix shows some remanent dislocation structures and numerous dislocation loops (upper left in Fig. 5b). It is also of interest to note the regular interphase boundary contrast at the Be particle/Al matrix interface in Fig. 5b (arrows). In addition, the Al matrix region is a continuous crystalline regime.

Figs 6 and 7 show TEM image features representative of the FSW zone. These TEM observations unambiguously demonstrate the implications of Figs 3b and 4: that the microstructure consists of intermixed, equiaxed, dynamically recrystallized grains of Al and Be. Fig. 6a and b show for comparison an alumium-rich polycrystalline area and a mixture of Al and Be grains, respectively. Fig. 7 shows a primarily Be-rich polycrystalline area in both bright and dark-field TEM. Taken together, Figs 6 and 7 correspond to the apparent stoichiometric mixtures implicit in Fig. 4c. It is especially interesting that the intermixing of Al and Be grains occurs in the recrystallized FSW zone because the melting points are considerably different as noted previously. Moreover, the fact that the Be recrystallizes in a size regime similar to the Al may be indicative that the recrystallization temperature might be around 500°C [5] rather than the 700 to 800°C range which is more usual for deformed Be.

The weld zone was observed to fail irregularly along the weld, especially at the leading (right) edge; with nugget segments fracturing at the weld base metal interface in a mixture of brittle-ductile fracture mode (predominantly ductile) features as illustrated typically in the SEM views of Fig. 8. Fig. 8 shows several examples of the fracture and fracture surface features characterizing the weld defects implict in Fig. 3a. There does not appear to be a dominant brittle fracture mode

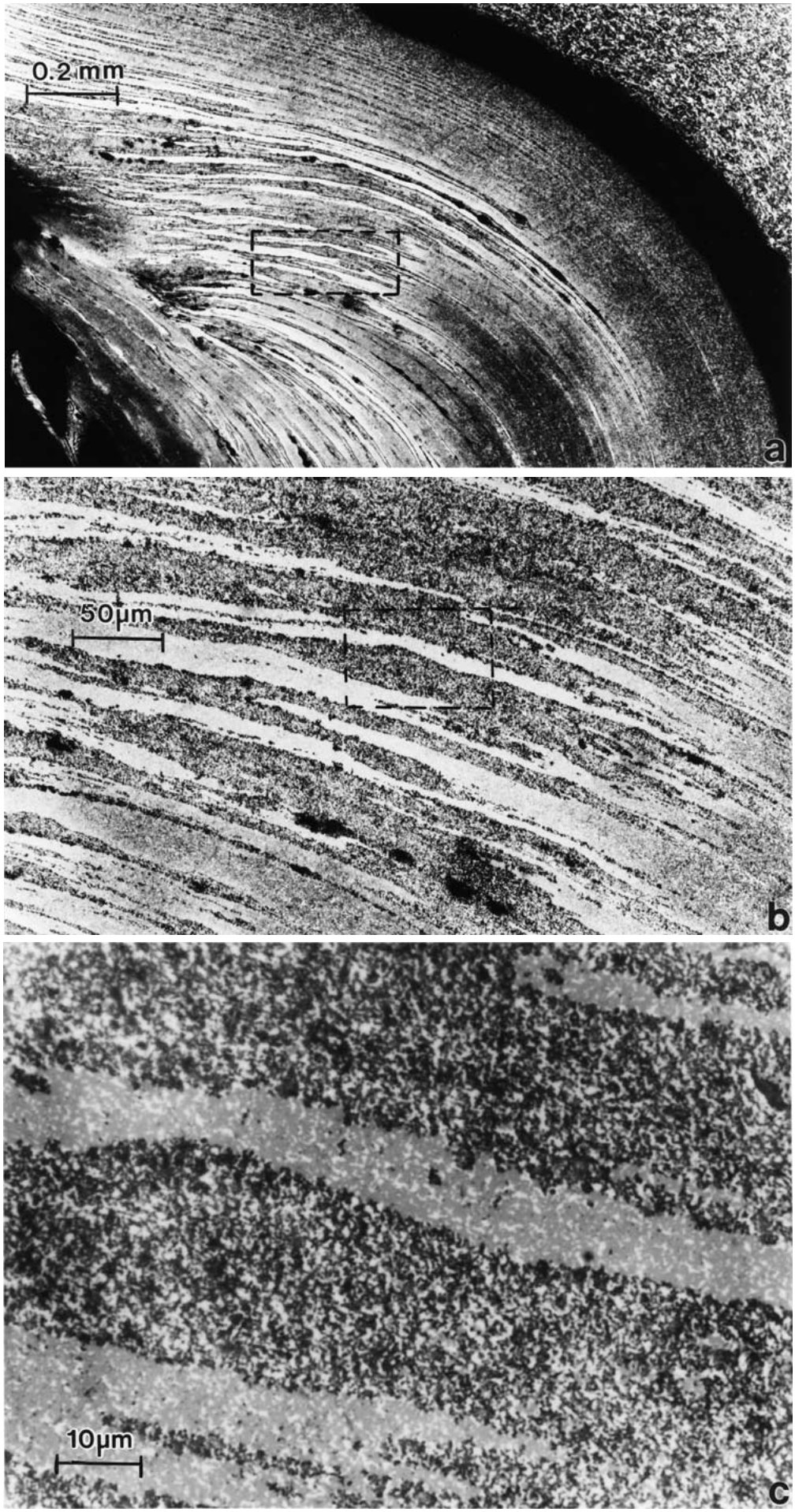

Figure 4 Progressive magnifications showing the compositional intercalation lamellae caused by variations in intermixed, recrystallized Al and Be grains. (a) FSW region in fractured nugget region (upper right in Fig. 3a). (b) Magnified view encircled in (a). (c) Magnified view encircled in (b).

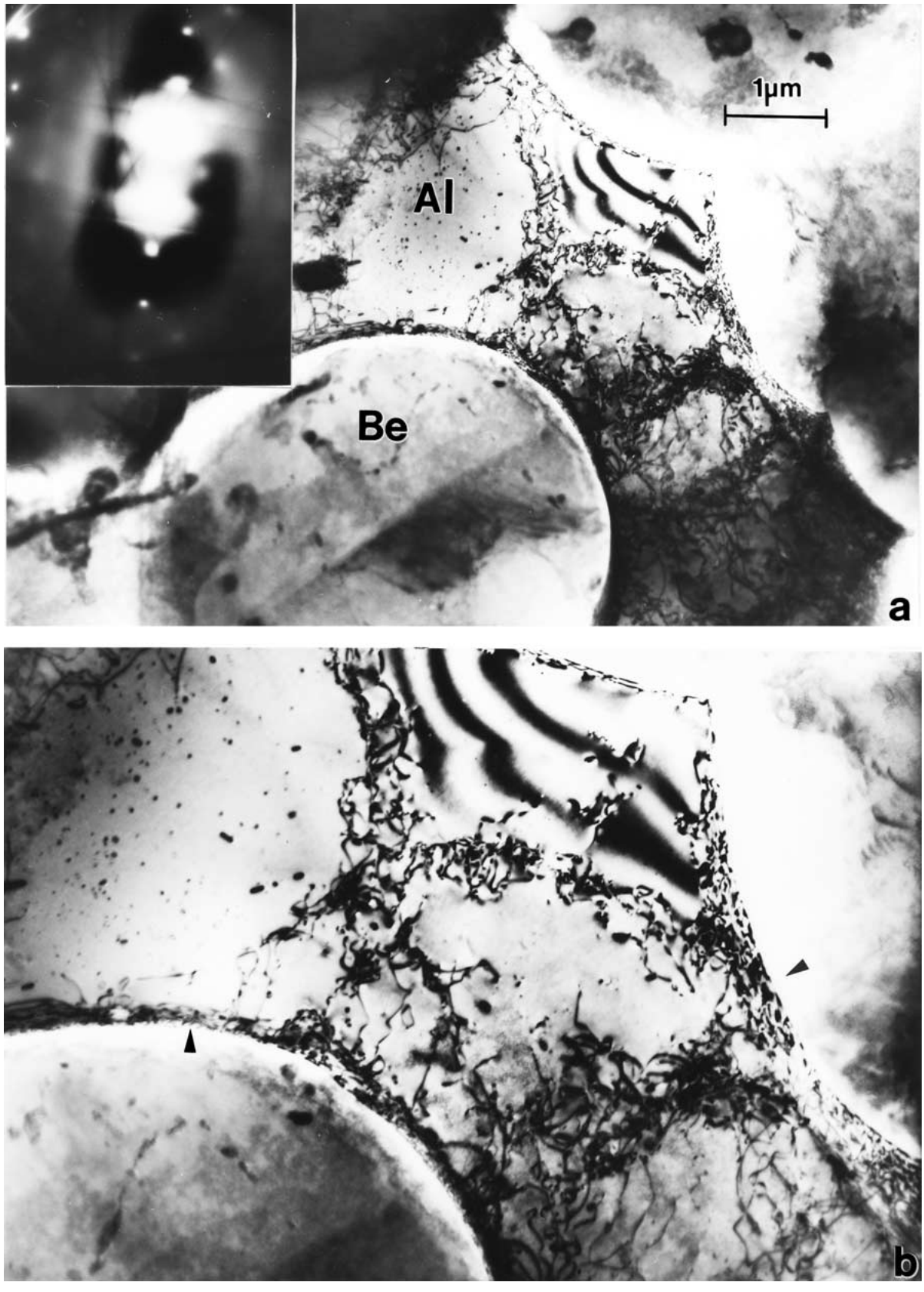

Figure 5 TEM views of microstructures in the FSW transition region (see Fig. 3b) for the Be 62-Al 38 composite. (a) Bright-field image showing Be particles in Al matrix. Selected-area electron diffraction pattern insert shows [110] aluminum matrix zone axis; $g = [004]$. (b) Magnified view of (a) showing the regular interphase boundary fringe contrast at the Be particle/Al matrix interface (arrows).

although there are regions of pronounced brittle fracture (Fig. 8a) and conchoidal-like (brittle) fracture (Fig. 8b); interspersed within more ductile shear-like transgranular features which characterize the majority of the fracture surfaces as shown in Fig. 8b and c. This appears to be indicative of a fairly uniform weld defect within the recrystallized beryllium/aluminum FSW zone composite. The ductile-cup and cone appearance typical for the very fine, recrystallized, interspersed Be and Al grains as shown in Fig. 8c has size features (0.5 μm to 3 μm)

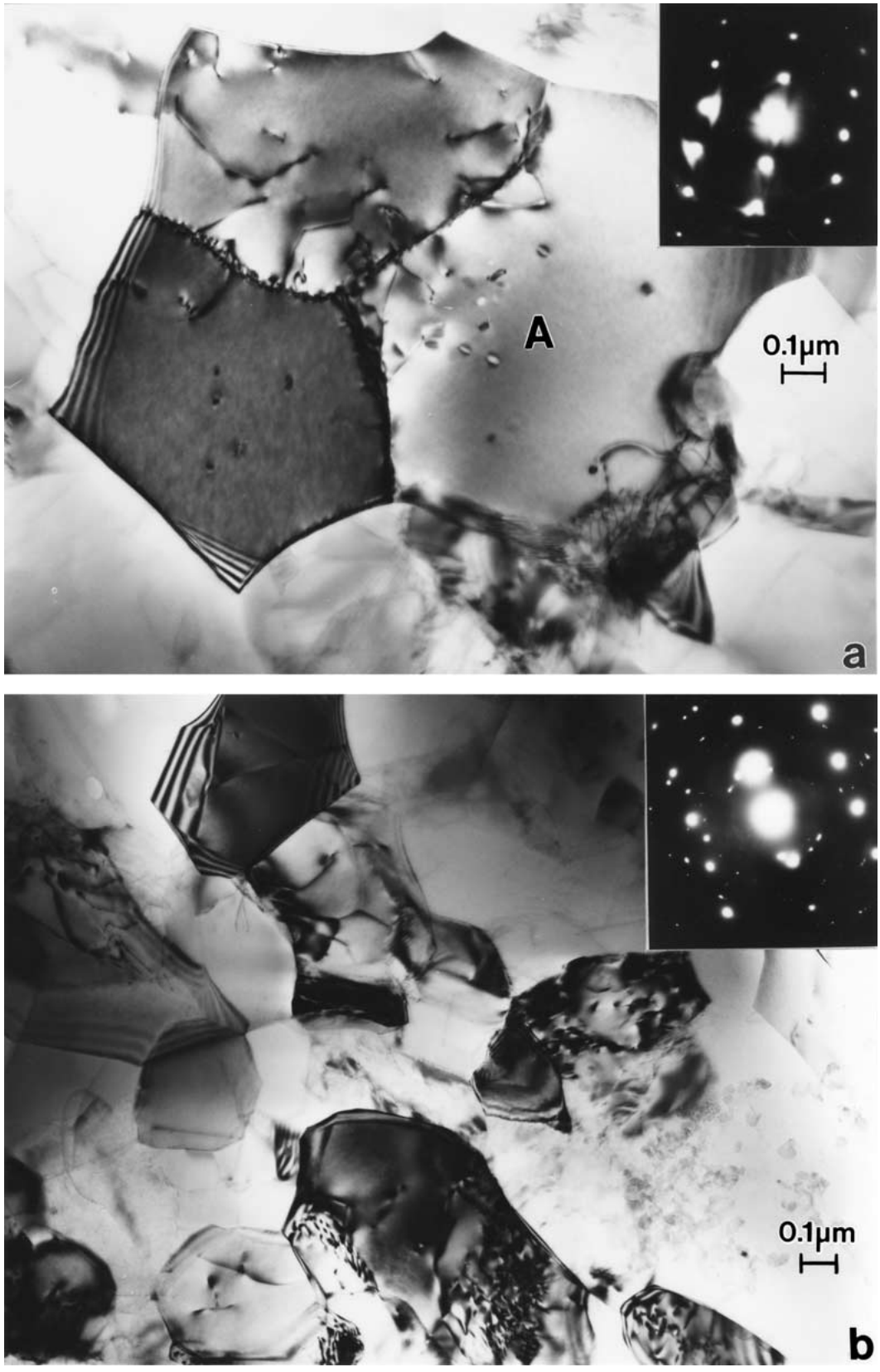

Figure 6 TEM observations showing the typical FSW zone microstructures. (a) Polycrystalline aggregate regime of primarily aluminum grains. The fcc [112] zone SAD pattern corresponds to the large grain area marked A. (b) Mixture of Al and Be grains. The SAD pattern insert illustrates both fcc Al and hcp Be reflections.

commensurate with the FSW zone recrystallized grain sizes.

The refined, recrystallized Be grains interspersed in Al grains within the FSW zone create a significant hardening due to the overall composite refinement. This feature is implicit in the hardness profile shown in Fig. 9a. The Be 62-Al 38 composite weld zone hardening in Fig. 9a is compared with the relatively constant hardness exhibited by the FSW of 1100 aluminum in Fig. 9b, and the significant hardness and strength reduction which occurs for many age-hardenable alloys, such as 2024 aluminum shown in Fig. 9c. In fact, the

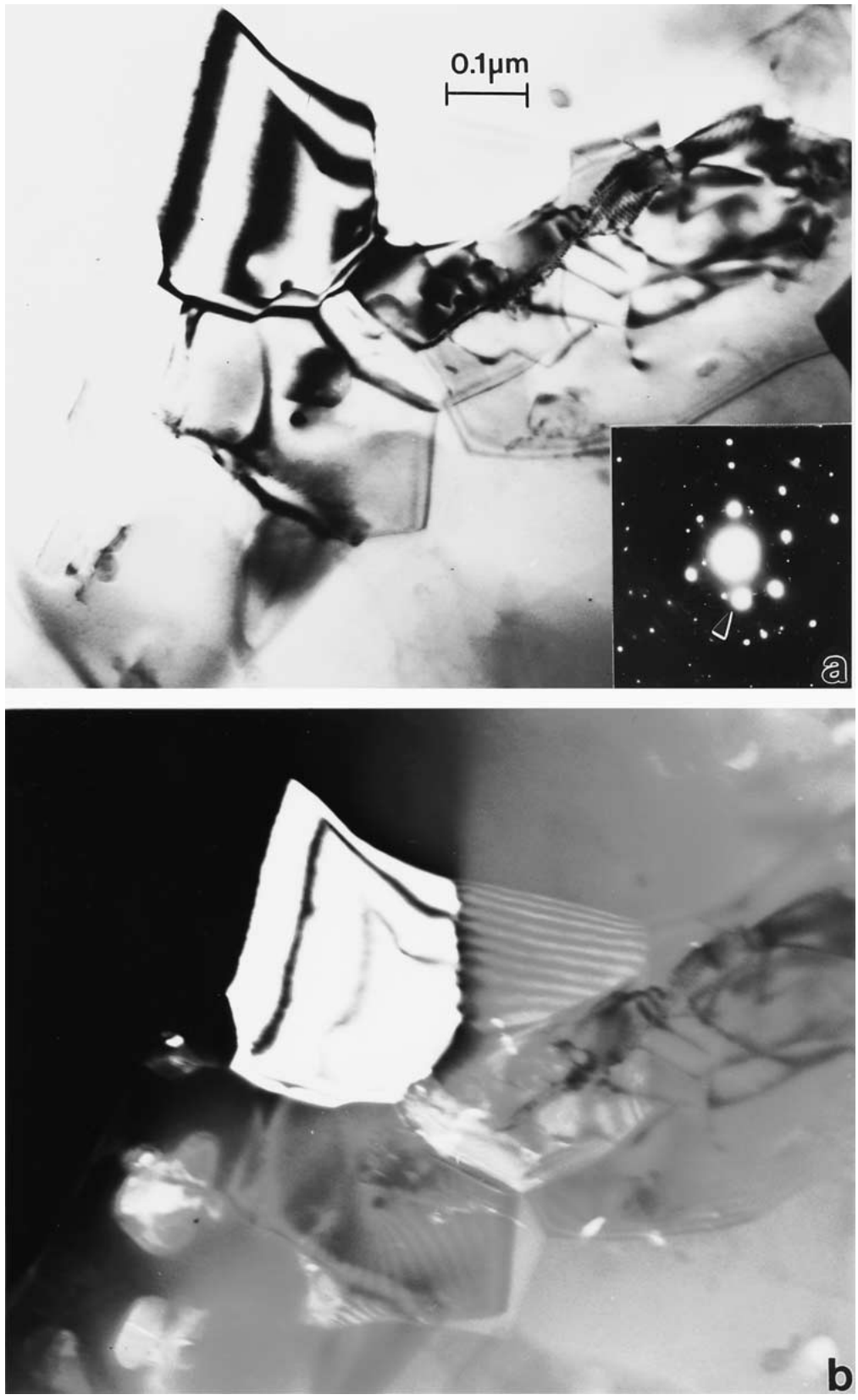

Figure 7 Predominantly Be polycrystalline regime in the FSW zone. (a) Bright-field TEM image. (b) Dark-field TEM image of (a) using the [0002] reflection in the $[10\bar{1}0]$ zone shown by arrow in the SAD pattern insert in (a). The SAD pattern insert in (a) is a mixture of $[10\bar{1}0]$ and $[11\bar{2}0]$ zone reflections. A weak $[11\bar{2}0]$ reflection is included in the dark-field image in (b) and corresponds to the weakly imaged grains.

FSW zone hardness increase in Fig. 9a is essentially identical to the hardness loss in Fig. 9c on a percentage basis $\Delta H \cong +115$ VHN versus $\Delta H \cong -60$ VHN or $+43\%$ versus -49%, respectively. The Be-Al MMC exhibits a base metal hardness slightly lower than the 2024 aluminum alloy. It is also interesting to note that the best thermal weld strength (for e-beam welding) of AlBeMet 162 sheet is only roughly 70 percent of the base metal (or -30%) [4].

The deformation of beryllium has been characterized as grain size dependent [9, 10] and Murr *et al*. [11] have shown that the grain boundary structure plays a

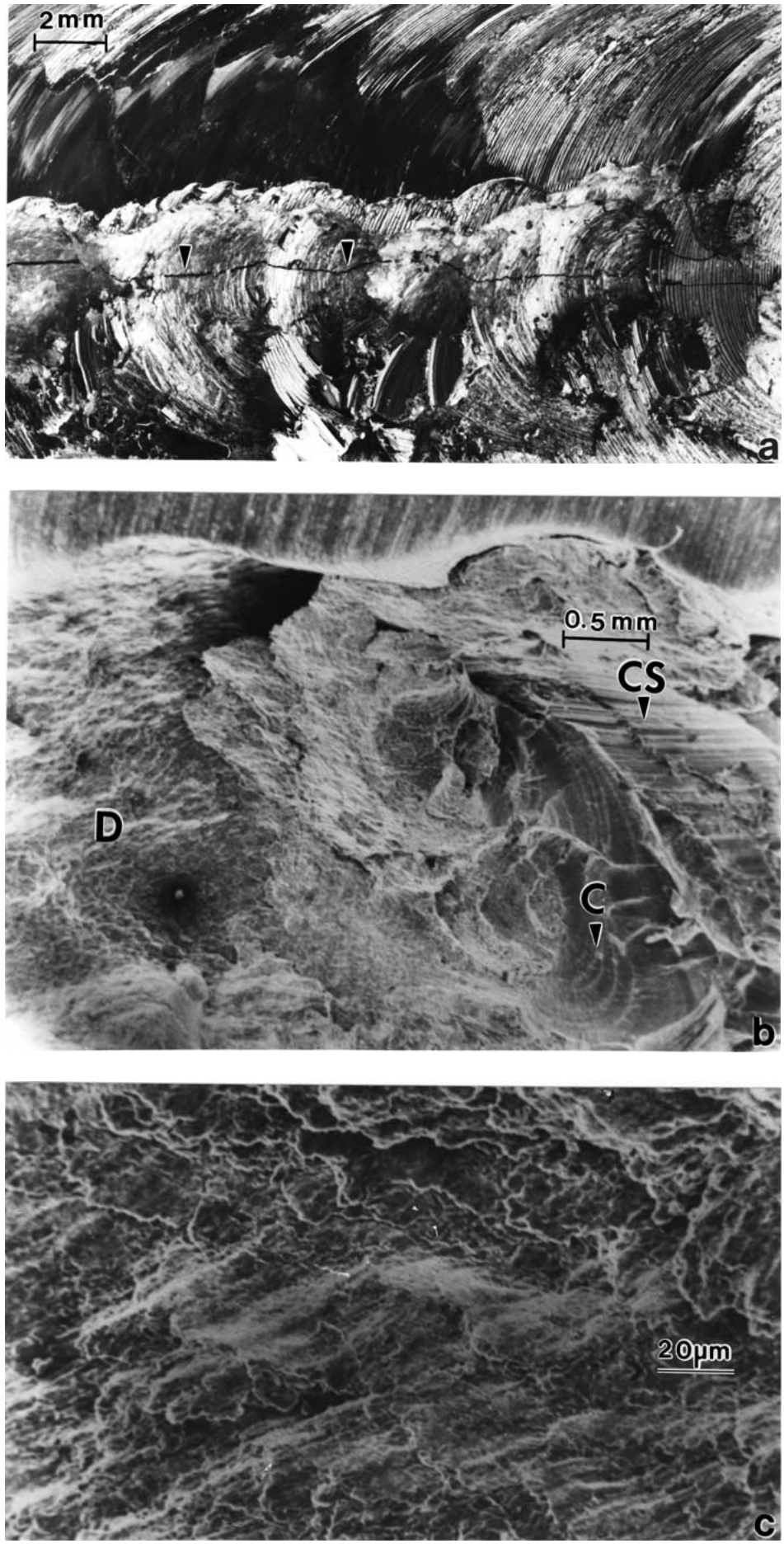

Figure 8 Fracture surface features along the FSW zone/base metal regime as observed in the SEM. (a) Top view (see Fig. 1) showing discontinuous failure and weld bead discontinuity. Arrows show brittle-like crack extending along the weld bead. (b) Magnified view at side of weld zone showing fracture surface features. D shows ductile-cup-cone shear failure regime while arrows show brittle, cleavage-like steps (CS) and concoidal, brittle regime (c). (c) Magnified view of ductile fracture features similar to D in (b).

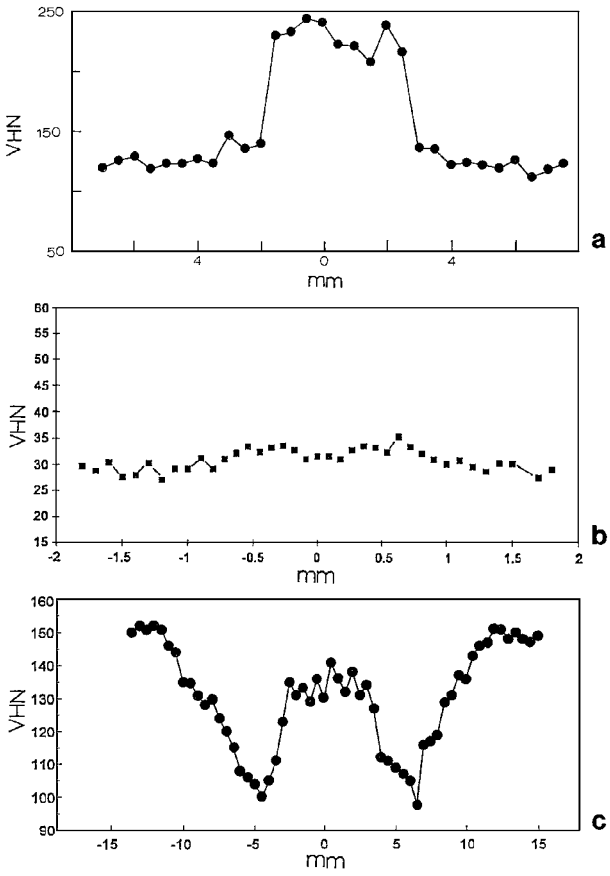

Figure 9 Comparison of the Be 62-Al 38 composite FSW zone residual microhardness profile (a) with those for 1100 Al (b) and 2024 Al (c). (b) and (c) are after reference [7].

role in the characteristic brittle fracture, especially for small grain sizes around 5 μm or less. This phenomenon also seems to play a role in the Be particle refinement, but the residual FSW microstructure is dominated by a very fine grain dispersion ($\sim$0.5 μm average size) of Be grains interspersed within the Al grains, or vice versa, although the Al grains tend to be somewhat larger than the Be grains on average. In fact Fig. 9a illustrates a friction-stir weld zone hardening which has only been observed previously in an aluminum 339-10% SiC MMC, where the aluminum alloy matrix is dynamically recrystallized and the grain size reduced from the base metal, while the SiC particles appear to be only slightly refined and stirred into the weld zone in a random fashion [5]. This SiC particle refinement appears to result by fracturing of small segments from larger particles and not involving any recrystallization except for the matrix. Correspondingly, the FSW of an aluminum 6061-20% Al_2O_3 MMC exhibits a reduction in hardening in the weld zone, but not as severe as that occurring for the FSW of 6061 aluminum which appears similar to that shown for 2024 aluminum in the data reproduced in Fig. 9c. Correspondingly, the AlBeMet 162 performs very much like a beryllium metal matrix composite especially in the FSW zone, and FSW poses a very promising joining process for aerospace and commercial applications where this material may find a variety of uses. Of course additional research trials will be necessary to optimize the FSW process, especially for varying dimensions and products to be welded (including hipped, extruded, or sheet products).

There is an additional processing issue implicit in the observations of Figs 3b to 8. That is, the PM Be-Al composite originally created in processing the base plate (Figs 2a and 3b) are refined and homogenized to create a uniform dispersion of essentially identical grains by a kind of mechanical alloying because there is no melting of the aluminum or beryllium. Consequently the continuous stirring of a region or regions within a plate of this material could create such homogenized regimes, which could have very novel features and consequences.

4. Summary and conclusions

The friction-stir welding of a beryllium metal matrix composite (AlBeMet 162), a primary beryllium powder phase in a continuous aluminum matrix, has been demonstrated. The FSW zone consists of a significantly recrystallized, refined dispersion of Be grains in recrystallized aluminum grains which gives rise to a hardness increase from the base metal of roughly 43 percent. This weld zone refinement (and grain and grain size homogenization) and hardening is somewhat characteristic of other MMC FSW behavior such as aluminum 339 + 10% SiC where there is some slight SiC refinement while the bulk of the SiC particles are randomly stirred into the weld zone. Similar to all other FSW processes there was no evidence of melting and no apparent release of airborne beryllium. Although this is a critical issue where more specific analysis must confirm this feature, the FSW process seems to provide a reduced potential for health risk. If the FSW process can be further optimized, it may be possible to join a variety of Be-Al alloys in a number of critical aerospace and commercial applications where high modulus, high thermal conductivity, low density, and a tailorable coefficient of thermal expansion may be simultaneously required.

Acknowledgements

This research was supported by a General Services Administration (GSA) Grant PF-90-018 as a component of a Materials Corridor Initiative research program with a focus on strategic materials issues at the University of Texas at El Paso. We are grateful for the technical support provided by David Brown.

References

1. I. STOL, *Welding J.* February (1994) 57.
2. http://www.matls.com/specificmaterial.asp; Brush Wellman AM 162 AlBeMet® Rolled Sheet, Annealed.
3. http://www.racetechmaj.com; GRID-Beryllium Engine Storm, p. 5, 1999.
4. T. PARSONAGE, *Mater. Sci. Technology* **16** (2000) 732.
5. L. E. MURR, YING LI, ELIZABETH A. TRILLO and J. C. Mc CLURE, *Mater. Tech. and Adv. Performance Mater.* **15**(1) (2000) 37.
6. YING LI, L. E. MURR and J. C. Mc CLURE, *Mater. Sci., Engng. A* **271** (1799) 213.

7. L. E. MURR, YING LI, ELIZABETH A. TRILLO, BROOKE M. NOWAK and J. C. Mc CLURE, *Aluminum Trans*. **1**(1) (1999) 141.
8. C. G. RHODES, M. W. MAHONEY, W. H. BINGEL, R. H. SPURLING and C. C. BAMPTON, *Scripta. Materialia* **36**(1) (1997) 69.
9. H. D. HANES, S. W. PORENSKO, J. B. McLEHAN and P. J. GRIPUHARA, Physical Metallurgy of Beryllium, Defense Metals Info. Center, Battelle Memorial Institute, Colombus, OH, DMCC Report 230, June 1966.
10. R. SCHMIDT, *Metals Progress* **86**(6) (1964) 132.
11. L. E. MURR, C-S. NIOU, A. H. ADVANI, L. VEGA, S. W. STAFFORD and J. M. HERRERA, *Mater. Sci. Engng.* **A151** (1992) 179.

Received 21 December 2000
and accepted 28 August 2001